Evaluation of Commercial Automotive-Grade BME Capacitors

Donhang (David) Liu
ASRC Federal Space and Defense, Inc.
NASA Goddard Space Flight Center
8800 Greenbelt Road, Greenbelt, Maryland 20771, USA
Donhang.liu-1@nasa.gov

Abstract

Three Ni-$BaTiO_3$ ceramic capacitor lots with the same specification (chip size, capacitance, and rated voltage) and the same reliability level, made by three different manufacturers, were degraded using highly accelerated life stress testing (HALST) with the same temperature and applied voltage conditions. The reliability, as characterized by mean time to failure (MTTF), differed by more than one order of magnitude among the capacitor lots. A theoretical model based on the existence of depletion layers at grain boundaries and the entrapment of oxygen vacancies has been proposed to explain the MTTF difference among these BME capacitors. It is the conclusion of this model that reliability will not be improved simply by increasing the insulation resistance of a BME capacitor. Indeed, Ni-$BaTiO_3$ ceramic capacitors with a smaller degradation rate constant K will always give rise to a longer reliability life.

Introduction

Ceramic capacitors with base-metal electrodes (BMEs) made with the same chip size, capacitance, and rated voltage, and that are qualified to the same reliability level, are expected to have similar usable life measurements that can statistically be characterized by mean time to failure (MTTF). However, actual measurements have shown that BME capacitors made to the same specifications (but made by different manufacturers) exhibit significant differences in their reliability performance.

These differences have posed a concern for the users of BME capacitors: when BME capacitors are procured per the same specifications, actual reliability differences must be evaluated to determine which manufacturers' products are more suitable for high-reliability applications. These evaluations are complicated by the lack of knowledge about the various formulation and processing conditions and background knowledge that different manufacturers employ when making BME capacitors qualified to reach certain levels of reliability. Since most of these design and processing parameters are considered proprietary by the manufacturers, it is possible that each manufacturer may use a different approach for making BME capacitors with the same reliability requirements.

The objective of this study is to gain insight into the key issues that may determine the reliability of BME capacitors, as this knowledge can be used to inform decisions about how to make

For publication on nepp.nasa.gov.

capacitors with improved reliability for possible space applications. A theoretical model based upon the oxygen vacancy migration and entrapment at grain boundary has been proposed to correlate the reliability, characterized by MTTF, and the depletion layer height reduction during the insulation resistance (IR) degradation in $BaTiO_3$ dielectric materials of BME capacitors.

Construction and Microstructure Characterizations

The microstructures of three BME capacitor lots from different manufacturers, AA47450, AB47450, and AC47450, were investigated by cross-section scanning electron microscope (SEM) to reveal the number of dielectric layers, average grain size, and average dielectric layer thickness. Typical cross-section SEM images of three BME capacitors are shown in Figure 1.

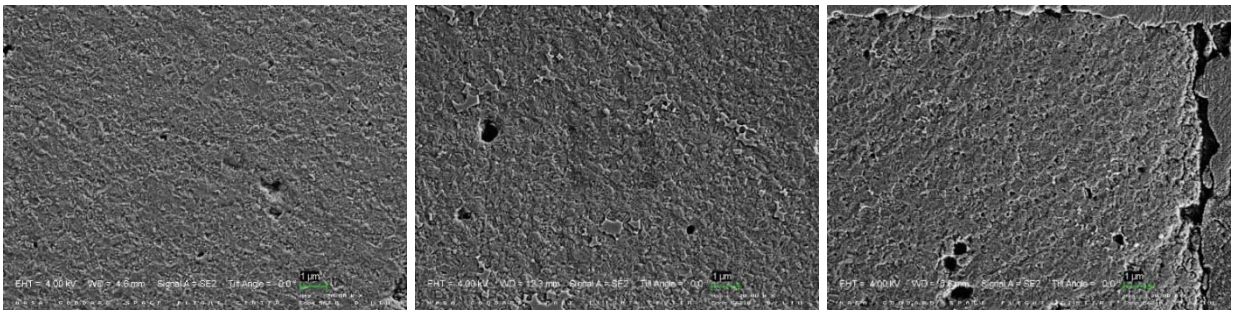

AA47450 AB47450 AC47450

Figure 1. Typical cross-section SEM images of the microstructure of three BME capacitors with the same specification and reliability level but made by three different manufacturers. There was no significant difference in dielectric layer thickness or average grain size.

Table I summarizes the specifications, number of dielectric layers, corresponding electrical field (V/thickness), and volts per grain at a given stress condition that will be used to degrade the capacitors to reveal their failure modes. The electric field can be determined by using the measured dielectric thickness and applied voltages. The volts per grain (the voltage to be applied on each individual $BaTiO_3$ grain) can be determined by using the dielectric thickness and measured average grain size information from the microstructure analysis.

The results in Table I show that at a given applied voltage, the volts per grain is nearly identical (less than 20% variation) among the three BME capacitor lots. It can be determined, then, that these capacitors are not only manufactured to the same specifications and reliability level, but they will also have a similar applied electrical strength during degradation.

Reliability Difference as Characterized by MTTF Data

After microstructure characterization, the three BME capacitor lots were degraded together using highly accelerated life stress testing (HALST) with the same temperature and applied voltage conditions, as shown in Table I. Twenty (20) BME capacitors were used for each stress condition. A 100 μA leakage current failure criterion was used across the board for all stress conditions. The leakage current of each capacitor sample as a function of stress time was recorded; this determines

the time to failure (TTF) of each capacitor. Figure 2 shows the leakage current against stress time for three BME capacitor lots at a given stress condition: 155°C, 250V (5x rated voltage). The plots in Figure 2 are made with the same scale on the x-axis. It can be seen that these capacitor lots, when degraded at the same stress condition, revealed significantly different TTF data!

Table I. Specifications and Calculated *E* (kV/mm), and Volts per Grain (V/Grain)

Part ID	Stress Level	E (kV/mm)	V/Grain
AA47450 0.47µF, 50V, 0805 Manufacturer A 98 layers $BaTiO_3$ thickness= 6.39 µm Ave. grain size= 0.38 µm	250V 175C	39.1236	14.75
	225V 165C	35.2113	13.27
	250V 165C	39.1236	14.75
	250V 155C	39.1236	14.75
	315V 155C	49.2958	18.59
AB47450 0.47µF, 50V, 0805 Manufacturer B 100 layers $BaTiO_3$ thickness= 5.80 µm Ave. grain size= 0.33 µm	250V 175C	43.0886	14.13
	225V 165C	38.7797	12.72
	250V 165C	43.0886	14.13
	250V 155C	43.0886	14.13
	315V 155C	54.2916	17.81
AC47450 0.47µF, 50V, 0805 Manufacturer C 103 layers $BaTiO_3$ thickness= 8.10 µm Ave. grain size= 0.40 µm	250V 175C	30.8642	12.45
	225V 165C	27.7778	11.20
	250V 165C	30.8642	12.45
	250V 155C	30.8642	12.45
	315V 155C	38.8889	15.68

A 2-parameter Weibull plot can be made when TTF data at a given stress level are available. The MTTF, a statistical parameter that measures the reliability, can be determined as:

$$MTTF = \eta\Gamma(1 + \beta^{-1}), \quad (1)$$

where slope β is the dimensionless shape parameter whose value is often characteristic of the particular failure mode, η is the scale parameter that represents the time at which 63.2% of the population has failed, and $\Gamma(x)$ is the gamma function of x.

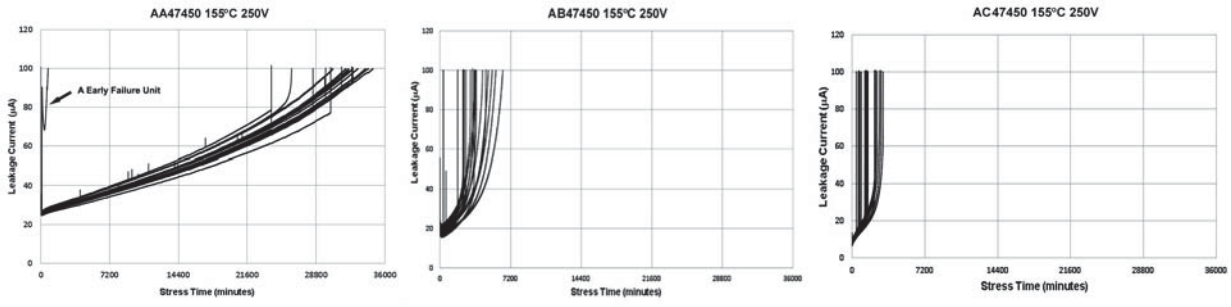

Figure 2. Leakage current as a function of stress time for three BME capacitor lots, degraded at 155°C, 250V. The plots were made with the same x-axis scale to reveal the difference in time-to-failure data.

Table II summarizes the calculated MTTF data using Eq. (1) when all TTF data at a given stress level were used to make a 2-parameter Weibull plot. The reliability life, as characterized by MTTF, was more than one magnitude in difference among the capacitor lots under the same stress condition.

Table II. Mean-Time-to-Failure Data of Three BME Capacitor Lots at Various Stress Conditions

	MTTF (Minutes) of BME Capacitors		
Test Conditions	AA47450	AB47450	AC47450
250V 175C	1466	450	319
250V 165C	9869	1140	626
225V 165C	15423	2066	1046
250V 155C	31602	3659	1479
315V 155C	17721	1102	648

Leakage Current Characterization

Why did these BME capacitor lots that were made to the same specifications and reliability level, and which degraded under almost identical stress conditions, vary so greatly with regard to reliability?

To answer this question, the leakage current data shown in Figure 2 were re-plotted with a different scale in the x-axis to reveal details of the differences in the failure modes. As shown in Figure 3, the TTF data appear to be highly dependent on the failure mode exhibited during the HALST regimen.

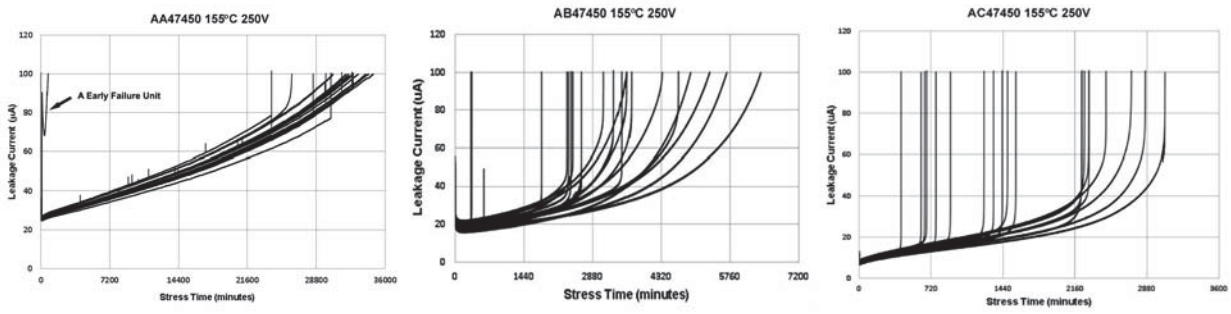

Figure 3. Leakage data shown in Figure 2, re-plotted with a different scale in the x-axis to reveal details in the failure modes among the three BME capacitor lots.

Two failure modes can be identified in these BME capacitor lots: catastrophic and slow degradation. A catastrophic failure is characterized by a time-accelerating increase in leakage current that is mainly due to existing processing defects (voids, cracks, delaminations, etc.) or to extrinsic defects. A slow degradation failure is characterized by a near-linear increase in leakage current against stress time; this is caused by the electromigration of oxygen vacancies (intrinsic defects) [1, 2]. The TTF data shown in Figure 3 clearly indicate that BME capacitors with slow

degradation failures have the largest MTTF values (AA47450), and those with catastrophic failures showed the smallest values (AC47450). Capacitor lot AB47450 shows failures with both failure modes.

As shown in Figure 3, for a certain period of stress time, the leakage current follows a similar degradation trend, characterized by a gradual increase in leakage current against stress time. With a further increase of stress time, some capacitors will fail catastrophically, while some will retain the near-linear increase of leakage current vs. stress time until the failure criterion is reached.

The leakage data shown in Figure 3 have been curved-fitted with a number of different functions (power law, exponential, linear, logarithmic, etc.). Although the leakage data shown in Figure 3 appear to be linear against most of the stress time measured, the curve-fitting results have shown that the exponential form of

$$I = I(t_0)e^{\left(\frac{t-t_0}{\tau_{SD}}\right)} \tag{2}$$

fits the leakage data better than a linear form. In Eq. (2), I is the measured leakage current, $I(t_0)$ is the leakage value at $t=t_0$, and τ_{SD} is a characteristic exponential growth time.

Figure 4 shows an example of curve fitting using Eq. (2) for two capacitor samples with different failure modes. C13, with a near-linear increase in leakage, fits very well to Eq. (2). Although C7 shows a catastrophic failure characterized by a rapid leakage current increase, the majority of the leakage data still fit well to Eq. (2), and a comparable τ_{SD} to that of C13 is obtained.

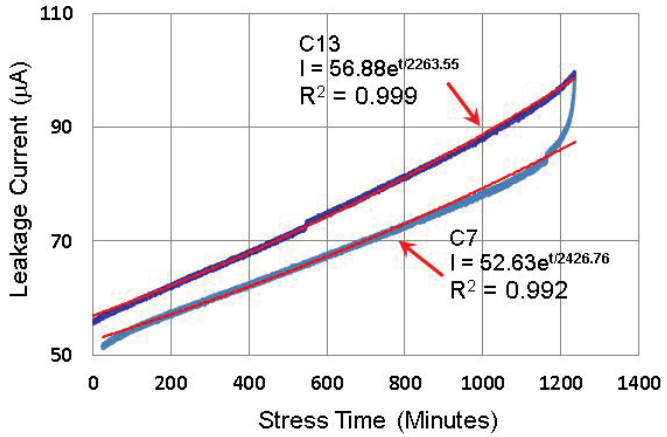

Figure 4. Examples of curve fitting using Eq. (2) for two BME B capacitor samples with different failure patterns. Both appear to fit well to the exponential form of Eq. (2).

By repeating the curve-fitting process shown in Figure 4, the characteristic growth time τ_{SD} can be experimentally determined for each capacitor unit under test. An average value of $<\tau_{SD}>$ can

be determined if all of the values of τ_{SD} under a given stress level are used to make a Weibull plot and $<\tau_{SD}>$ is simply the value of η of the Weibull plot.

Table III summarizes the values of $<\tau_{SD}>$ determined for various stress conditions and can be used to compare the corresponding MTTF data. In most cases, the value of $<\tau_{SD}>$ was greater than that of MTTF, but it was smaller in a few lower-stress levels where the catastrophic failure mode is dominant.

Table III. Calculated MTTF Data from Weibull Plots and Calculated $<\tau_{SD}>$ of the Three BME Capacitor Lots at Various Degradation Conditions

	MTTF (Minutes)	$<\tau_{SD}>$ (Minutes)
Test Conditions	AA47450	
250V 175C	1466	3333
250V 165C	9869	11111
250V 155C	31602	34925
Test Conditions	AB47450	
250V 175C	450	667
250V 165C	1140	1714
250V 155C	3659	3333
Test Conditions	AC47450	
250V 175C	319	357
250V 165C	626	769
250V 155C	1479	1667

The meaning of τ_{SD} can be illustrated by the following example: Let I_1 and I_2 be the leakages at t_1 and t_2, respectively, for a slow degradation failure. If one assumes $\frac{I_2}{I_1} = 2$, then Eq. (1) can be rewritten as:

$$\frac{I_2}{I_1} = e^{\left(\frac{t_2 - t_1}{\tau_{SD}}\right)} = e^{\left(\frac{\Delta t}{\tau_{SD}}\right)} = 2$$

and

$$\tau_{SD} = \frac{\Delta t}{ln(2)} \approx 1.4427 \cdot \Delta t, \quad (3)$$

where Δt is the time at which the leakage current doubles in value. The greater the value of τ_{SD}, the longer the timespan of a degradation failure, indicating a slower degradation process.

A Degradation Model for BME Capacitors

1. Time-dependent depletion layer height $\phi(t)$

Although the formation of a double Schottky barrier layer at a grain boundary, as shown in Figure 5, was initially proposed to explain the positive temperature coefficient of resistance (PTCR) effect in donor-doped semiconducting $BaTiO_3$ ceramics [3-5], the same barrier depletion layer model

has also been suggested to explain the IR degradation in Ni-$BaTiO_3$ ceramic capacitors [6, 7]. The typical barrier height can be expressed as

$$\phi = \frac{e^2 N_d d^2}{2\varepsilon_0 \varepsilon_r},$$

where N_d is the donor concentration, d is the depletion layer thickness, e is the electron charge, and $\varepsilon_0 \varepsilon_r$ is the dielectric constant. The electro-neutrality condition in the depletion layer satisfies the following condition [3]:

$$d = \frac{n_s}{2N_d}, \tag{4}$$

where n_s is the concentration of trapped electrons at grain boundary acceptor states (cm^{-2}). The ϕ can be re-written as

$$\phi = \frac{e^2 n_s^2}{8\varepsilon_0 \varepsilon_r N_d}. \tag{5}$$

Eq. (5) often has been used to estimate the grain boundary barrier height in semiconducting $BaTiO_3$ ceramics [8, 9]. In Ni-$BaTiO_3$ ceramic capacitors, N_d is mainly determined by the bulk concentration of ionized oxygen vacancies. The value of d in Eq. (4) is often in the submicron range, indicating that $N_d >> n_s$. One can then assume that $N_d(t) \approx N_d(0)$, and that it is independent of time. Therefore,

$$\frac{d\phi(t)}{dt} = \frac{d}{dt}\left(\frac{e^2 n_s^2}{8\varepsilon_0 \varepsilon_r N_d}\right) = \frac{e^2}{4\varepsilon_0 \varepsilon_r N_d}\left(\frac{dn_s(t)}{dt}\right).$$

In order to determine $\left(\frac{dn_s(t)}{dt}\right)$, the following facts were considered: 1) $n_s(t)$ is trapped electrons at surface acceptor states in the grain boundary regions. As shown in Figure 3, the negative space charge due to trapped electrons is compensated for by the formation of a positive space charge region near the grain boundary, which behaves like a depletion barrier layer to electron conduction. 2) The computational analysis on the trapping of oxygen vacancies at grain boundaries with respect to local atomic configuration and energy shows that grain boundaries attract oxygen vacancies and trap them at specific sites at which local cation density is lower than in the grain interior [10]. 3) Since oxygen vacancies behave like donors, they possess positive space charges when ionized. The same positive space charge in a barrier layer at a grain boundary will thus act as a resistance for positively charged oxygen vacancy diffusion in a polycrystalline $BaTiO_3$ dielectric. As a result, when an ionized oxygen vacancy migrates under a DC field and reaches the barrier layer, it has a tendency to become trapped there. The electro-neutrality condition requires that the weakly bonded two electrons that are moving in a conduction band now have to be localized in order to make the trapped oxygen vacancy electrically neutralize and become part of the crystalline structure. When Kroger and Vink symbols are used [11], the process can be simply described by

$$V_O^{\bullet\bullet} = V_O + 2e'. \tag{6}$$

As previously reported, the localized electrons that are necessary to offset the $V_O^{\bullet\bullet}$ localization can be trapped with the reduction of *Ti* ions surrounding the $V_O^{\bullet\bullet}$ as $Ti^{4+} + e' \rightarrow Ti^{3+}$ and $Ti^{3+} + e' \rightarrow Ti^{2+}$[7]. The reduction of Ti^{4+} will now reduce the positive space charge in the positively charged depletion layer and then reduce the barrier height. Since the barrier height is balanced by the trapped electrons in surface acceptor states $n_s(t)$, the reduction in barrier height will lower the Fermi level at grain boundary and reduce the $n_s(t)$.

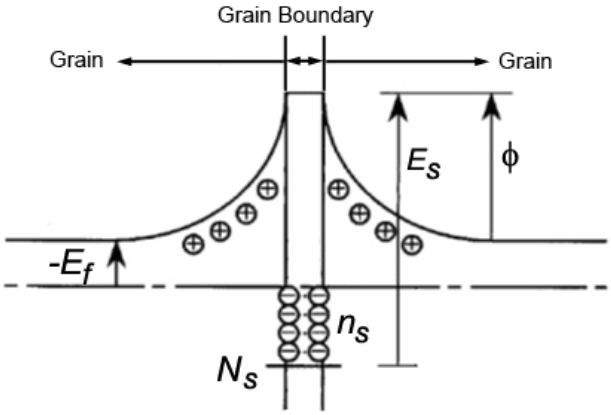

Figure 5. Schematic illustration of the formation of a double Schottky barrier around the grain boundary of a $BaTiO_3$ ceramic capacitor.

If we assume that Δn_O is the electron concentration that has been localized to make the trapped $V_O^{\bullet\bullet}$ neutral, Δn_O should meet the following conditions: at $t = 0$, $\Delta n_O(0) = 0$, and at $t \rightarrow \infty$, $\Delta n_O = n_s(0)$, i.e., all trapped electrons at $t = 0$ in the surface acceptor states $n_s(0)$ will eventually be fully electrically balanced by the localized electrons that neutralize the trapped $V_O^{\bullet\bullet}$. However, with a further increase of Δn_O as more $V_O^{\bullet\bullet}$ are trapped and neutralized, the electrically negative feature of $n_s(t)$ will further retard the localization of electrons and reduce the localization rate of Δn_O. Therefore, the change of Δn_O as a function of *t* can be expressed by a first-order reaction according to the reaction rate theory [12]

$$\frac{d\Delta n_O(t)}{dt} = K(t)[n_s(0) - \Delta n_O(t)]$$

and

$$\int_{\Delta n_O(0)}^{\Delta n_O(t)} \frac{d\Delta n_O(t)}{\Delta n_O(t) - n_s(0)} = \int_0^t -K(t)dt \tag{7}$$

where *K(t)* is called the degradation rate constant and $n_s(0) - \Delta n_O(t) = n_s(t)$ is the trapped electron concentration at surface acceptor states at time *t*. If $\Delta n_O(t)$ is only balanced by $n_s(t)$ near

the Fermi level, $K(t) = K = K_0 e^{-\frac{E_k}{kT}}$ can be simplified as a time-independent constant, where E_k is the activation energy that is required for $V_O^{\bullet\bullet}$ to electromigrate and to be neutralized at a grain boundary region per Eq. (6), where *k* is the Boltzmann constant. Since $\Delta n_O(0) = 0$, Eq. (7) finally yields

$$\frac{n_s(0) - \Delta n_O(t)}{n_s(0)} = e^{-\mathrm{K}t}$$

and

$$\Delta n_O(t) = n_s(0)(1 - e^{-\mathrm{K}t}). \tag{8}$$

The remaining trapped electrons in acceptor states can be simply expressed according Eq. (8) as

$$n_s(0) - \Delta n_O(t) = n_s(0) - n_s(0)(1 - e^{-\mathrm{K}t}) = n_s(0)e^{-\mathrm{K}t}.$$

Combining Eqs. (5) and (8) yields a time-dependent barrier height

$$\phi(t) = \frac{e^2[n_s(0) - \Delta n_O(t)]^2}{8\varepsilon_0 \varepsilon_r N_d} = \phi(0)\mathrm{e}^{-2\mathrm{K}t}. \tag{9}$$

This relationship indicates that the barrier height will exponentially decrease with time due to the oxygen vacancy migration and localization at grain boundaries.

2. Determination of degradation rate constant *K*

The measurement of I-V characteristics of ceramic $BaTiO_3$ inside the grain interior and at the grain boundary has shown that under an applied field of 100 kV/cm, the current density inside the grain and at the grain boundary can differ by several orders of magnitude. The difference increases significantly as temperature increases [13]. In a Ni-$BaTiO_3$ ceramic capacitor, it is the grain boundary that holds the high dielectric resistivity of the ceramic $BaTiO_3$. If all grain boundaries inside a dielectric layer are assumed to have a uniform barrier height $\phi(t)$, the time-dependent resistivity $\rho(t)$ of a BME ceramic capacitor can be simply written as

$$\rho(t) = \rho_0 e^{\left(\frac{\phi(t)}{kT}\right)}, \tag{10}$$

where ρ_0 is the resistivity of the grain. According to Eq. (1), the time-dependent current density of a BME capacitor $j(t) = A \times I(t)$ can be expressed as

$$j(t) = j(t_0)e^{\left(\frac{t-t_0}{\tau_{SD}}\right)} = \frac{E}{\rho(t)}$$

or

$$\rho(t) = \frac{E}{j(t_0)} e^{-\left(\frac{t-t_0}{\tau_{SD}}\right)}, \tag{11}$$

where $j(t_0)$ is the current density at $t = t_0$, E is the applied field, and A is the cross-section area for current flow. Combining Eqs. (10) and (11) results in

$$\rho(t) = \rho_0 exp\left(\frac{\phi(t)}{kT}\right) = \rho_0 exp\left(\frac{\phi(0)\mathrm{e}^{-2\mathrm{Kt}}}{kT}\right) = \frac{E}{j(0)} exp\left(-\frac{t-t_0}{\tau_{SD}}\right).$$

At a given stress level, *E* is a constant, so that

$$e^{\frac{t-t_0}{\tau_{SD}}} \approx e^{-\frac{\phi(0)}{kT}\mathrm{e}^{-2\mathrm{Kt}}}. \quad (12)$$

Using $\langle\tau_{SD}\rangle$, the average of τ_{SD}, to replace τ_{SD}, and $e^{-x} \approx 1 - x$ when *x* is small, the integration of the exponential part of Eq. (12) results in:

$$\int_0^{MTTF} \frac{t-t_0}{\langle\tau_{SD}\rangle} dt = -\int_0^{MTTF} \frac{\phi(0)}{kT} \cdot \mathrm{e}^{-2\mathrm{Kt}} dt \approx -\int_0^{MTTF} \frac{\phi(0)}{kT}(1-2Kt)dt$$

and

$$\frac{1}{2\langle\tau_{SD}\rangle} \approx \frac{\phi(0)}{kT}\left(K - \frac{1}{MTTF}\right).$$

This gives rise to

$$\frac{1}{MTTF} = K - \frac{kT}{2\phi(0)\langle\tau_{SD}\rangle} \approx K_0 e^{-\frac{E_k}{kT}}. \quad (13)$$

Eq. (13) is the Prokopowicz-Vaskas equation where applied voltage is a constant [14]. The degradation rate constant *K* can now be simply determined by an Arrhenius plot using the MTTF data obtained at various temperatures and at a constant voltage.

Using the MTTF data at different temperatures and a given voltage (250V) for three BME capacitor lots, a corresponding Arrhenius plot according to Eq. (13) can be plotted, as shown in Figure 6. The activation energy E_k and degradation rate constant *K* can both be calculated.

Table IV lists the activation energy E_k and constant *K* at two different temperatures for three BME capacitor lots. The calculated *K* values shown in Table IV are used to estimate the MTTF data per Eq. (13). The comparison between the measured MTTF data and the calculated data shows fairly good agreement. All calculated MTTF values are smaller than the measured ones. For lot AA47450, the MTTF data measured at 175°C were excluded for the estimation of the degradation rate constant K because its value is much smaller when combined with other MTTF data points to give rise to a good linear fitting. Since the units are so leaky at this temperature, the results of self-heating due to the leakage current could result in a significant amount of temperature increase and thus an acceleration of the failure of the BME capacitors.

3. IR degradation mechanism due to oxygen vacancy electromigration

3.1. Reliability and oxygen vacancy migration

According to Eq. (9),

$$\phi(t) = \phi(0)\mathrm{e}^{-2\mathrm{Kt}} = \phi(0)\mathrm{e}^{-\frac{2\mathrm{t}}{MTTF}},$$

where $K = K_0 e^{\frac{-E_k}{kT}}$ is the degradation rate constant for oxygen vacancy entrapment at grain boundaries. Although K and MTTF can be related to each other per the Prokopowicz-Vaskas equation, the meaning of K was clearly defined in the proposed model. To make Ni-$BaTiO_3$ BME capacitors with improved reliability, the value of K must be minimized. This requires a smaller value of the degradation constant K_0 or a large value of E_k, which is the activation energy required for $V_O^{\bullet\bullet}$ to migrate and to be neutralized near the depletion layer at grain boundaries. This has been proven from the calculated K values shown in Table IV, where AA47450 and AB47450 are shown to have similar values of E_k but a much smaller value for K_0, which gives rise to a significantly large MTTF for lot AA47450.

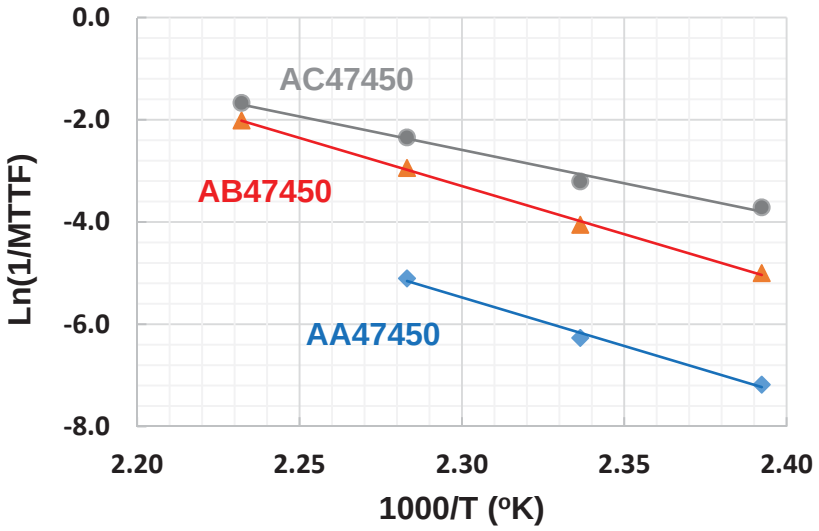

Figure 6. Arrhenius plots using Eq. (13) and measured MTTF data in Table II for three BME capacitor lots.

Table IV. Calculated Degradation Constant and MTTF data per the Curve-Fitting Results in Figure 6 and Eq. (13)

	$K_0 e^{\frac{-E_k}{kT}}(hour^{-1})$			MTTF (minutes) at 155°C, 250V	
Capacitor ID	E_k (eV)	at 398K (125°C)	at 428K (155°C)	Measured	Calculated
AA47450	1.65	$7.38\text{x}10^{-5}$	$2.10\text{x}10^{-3}$	31602	28640
AB47450	1.63	$6.76\text{x}10^{-4}$	$1.86\text{x}10^{-2}$	3459	3218
AC47450	1.11	$4.94\text{x}10^{-3}$	$4.73\text{x}10^{-2}$	1479	1268

On the other hand, since a typical barrier height value of $\phi(0) \approx 1.30$ eV has been reported previously [7], a large value of $E_k > \phi(0)$ is necessary to slow down the $V_O^{\bullet\bullet}$ entrapment, because

a large value of E_k also means that the entrapment of $V_O^{\bullet\bullet}$ at grain boundaries may not be an energetically favorable process unless the barrier height $\phi(t)$ is high enough to be comparable to E_k. This is the case for AC47450, where E_k=1.11 eV is smaller than that of $\phi(0)$.

Finally, since $N_d \gg n_s$ per Eq. (4), only a tiny fraction of oxygen vacancies can be trapped at the grain boundaries during the electromigration across the dielectric layer to cause IR degradation. This indicates that the effort to simply reduce the level of $V_O^{\bullet\bullet}$ in the dielectric material would not significantly slow down the IR degradation.

3.2. Reliability and insulation resistance

According to Eq. (12),

$$e^{\frac{t-t_0}{\tau_{SD}}} \approx e^{-\frac{\phi(0)}{kT}e^{-2Kt}},$$

which indicates that a slower degradation, characterized by a larger value of τ_{SD}, would give rise to a smaller value of $\phi(0)$. This makes sense since a smaller $\phi(0)$ will energetically be favorable to the continuous electromigration of $V_O^{\bullet\bullet}$ without being trapped or localized at a grain boundary to cause an IR degradation. However, this is only one part of the equation; $\phi(0)$ also presents the barrier height for the conduction band electron carriers. A lower $\phi(0)$ will facilitate electron conduction and will also deteriorate the IR. As a result, when electron conduction and oxygen vacancy electromigration are both taken into account, a moderate barrier height and a smaller *K* are the keys for minimal IR degradation in Ni-$BaTiO_3$-based ceramic capacitors.

As an important conclusion of this model development, higher IR values may not always result in a larger MTTF, but a slower IR degradation rate (smaller *K*) will always do. This conclusion can be verified from the measured leakage data shown in Figure 3, where sample AC47450 was shown to have the highest initial IR values and smallest MTTF and AA47450 had the lowest initial IR values but the largest MTTF among the group.

A higher $\phi(0)$ generally means a higher resistance and therefore a higher electrical strength when a DC voltage is applied. This highly localized electric strength is more likely to cause the thermally related electrical breakdown of the depletion layer and a reduction in the reliability life of the ceramic capacitors [15-17].

3.3. Oxygen vacancy migration and compensation

Since only a very small portion of $V_O^{\bullet\bullet}$ may be trapped at the grain boundaries, the majority of $V_O^{\bullet\bullet}$ will continually migrate and will eventually reach the dielectric layer and internal Ni electrode interface, as has been shown by previously reported electron energy loss spectroscopy (EELS) and high-resolution transmission electron microscope (HRTEM) observations [7].

Since there is no evidence to show that $V_O^{\bullet\bullet}$ can be transferred across the cathode electrode layer [7, 16], most $V_O^{\bullet\bullet}$ capable of migration will now pile up along the Ni-electrode dielectric interface.

To neutralize these vacancies, a significant number of electrons is required, which can only be obtained from the cathode electron injection. The energy required for cathode electron injection at the dielectric-electrode interface is ~1.25 eV [18]. If E_k is less than this value, most of the oxygen vacancies will be energetically favorable for a localization and a quick IR degradation will occur. This is exactly the case for lot AC47450.

The high concentration of localized electrons due to the compensation of the pile-up of oxygen vacancies will not only dramatically change the local stoichiometry of the $BaTiO_3$ dielectric, but it will also lead to a leakage current increase during IR degradation. This will cause a local temperature increase and will eventually lead to the breakdown at the Ni-$BaTiO_3$ interface. The initial failure site of the dielectric-electrode interface was revealed in a previously published failure analysis work regarding commercial BME ceramic capacitors [19].

Summary

Three BME capacitor lots with the same specification (chip size, capacitance, and rated voltage) and reliability level, made by three different manufacturers, were selected for reliability performance evaluation. The microstructure analysis of these capacitors showed that the three BME products had a similar number of dielectric layers and a similar number of grains per dielectric layer. When an external voltage was applied, the volts per grain was almost identical for these capacitors, indicating that the dielectrics will experience the same voltage stress when electrically tested under the same externally applied voltages.

These BME capacitors were then degraded using highly accelerated life stress testing (HALST) with the same temperature and applied voltage conditions. The reliability performance, as characterized by MTTF, differed by more than one order of magnitude among the capacitor lots.

A model based on the existence of depletion layers at grain boundaries and the entrapment of oxygen vacancies has been proposed to explain the MTTF difference among these BME capacitors. The MTTF is directly related to the degradation rate constant K of the entrapped oxygen vacancies. The MTTF and K were found to follow the traditional Prokopowicz-Vaskas equation at a constant applied voltage.

A lower depletion layer height $\phi(0)$ is energetically favorable for a slower degradation rate and a longer reliability life. However, when both oxygen vacancy migration and electronic conduction are taken into account, the $\phi(0)$ with a moderate height would give rise to the best reliability performance.

It is the conclusion of this study that reliability will not be improved simply by increasing the insulation resistance. Indeed, Ni-$BaTiO_3$ BME capacitors with a smaller IR degradation rate constant K will always give rise to an improved reliability life.

Acknowledgements

The author appreciates the NASA Electronic Parts and Packaging (NEPP) program's support for this study. The author also expresses his gratitude to Michael Sampson and Bruce Meinhold for reviewing the manuscript. The author would also like to thank the GSFC Code 562 Parts Analysis Laboratory for assistance with electrical testing.

References

[1] D. Liu and M. Sampson, CARTS Proceedings, Las Vegas, NV, pp. 59-71, March 2012.
[2] D. Liu, CARTS Proceedings, Houston, TX, pp. 235-248, March 2013.
[3] W. Heywang, J. Am. Ceram. Soc., vol.47, no.10, pp.484-490, October 1964.
[4] G. Jonker, Solid-State Electron. vol.7, pp. 895-903, July 1964.
[5] G. Jonker, Mat. Res. Bull., vol.2, no.4, pp. 401–407, April 1967.
[6] H. Chazono and H. Kishi, Jpn. J. Appl. Phys., Part 1, vol.40, no.9B, pp. 5624–5629, September 2001.
[7] G. Y. Yang, G. D. Lian, E. C. Dickey, and C. A. Randall, D. E. Barber, P. Pinceloup, M. A. Henderson, R. A. Hill, J. J. Beeson, and D. J. Skamser, J. Appl. Phys., vol.96, no.12, pp. 7500-7508, December 2004.
[8] E. Brzozowski and M. Castro, J. European Ceramic Society, vol.24, no.8, pp. 2499–2507, July 2004.
[9] J. Illingsworth, H. AI-Allak, and A. Brinkman, J. Phys. D: Appl. Phys., vol.23, no.7, pp. 971-975, July 1990.
[10] T. Oyama, N. Wada, H. Takagi, and M. Yoshida, Phys. Rev. B, vol.82, no.13, pp.134107-134116, July 2010.
[11] F. Kröger and H. J. Vink, Solid-State Physics, vol.3, pp. 307–435, March 1956.
[12] K. Connors, *Chemical Kinetics, the study of reaction rates in solution*, VCH Publishers, New York, 1991.
[13] T. Nakamura, T. Yao, J. Ikeda, N. Kubodera, and H. Takagi. *IOP Conference Series: Materials Science and Engineering*, vol.18, no.9, pp.092007-092012, IOP Publishing, 2011.
[14] T. I. Prokopowicz and A. R. Vaskas, Final Report ECOM-90705-F, NTIS AD-864068, October 1969.
[15] R. Waser, J. Am. Ceram. Soc., vol.72, no.12, pp. 2234-2240, December 1989.
[16] R. Waser, T. Baitu, and K.H. Härdtl, J. Am. Ceram. Soc., vol.73, no.6, pp.1645-1653, June 1990.
[17] R. Waser, T. Baiatu, and K. H. Härdtl, J. Am. Ceram. Soc., vol.73, no.6, pp.1654-1662, June 1990.
[18] A. Polotai, I. Fujii, D. Shay, G. Yang, E. Dickey, and C. Randall, J. Am. Ceram. Soc., vol.91, no.8, pp. 2540-2544, Aug. 2008.
[19] R. Weachock and D. Liu, CARTS Proceedings, Houston, TX, pp. 151-165, March 2013.